Emberson, R., Hovius, N., Galy, A., Marc, O. (2016): Chemical weathering in active mountain belts controlled by stochastic bedrock landsliding. - *Nature Geoscience*, *9*, pp. 42—45.

DOI: http://doi.org/10.1038/ngeo2600

Chemical weathering in active mountain belts controlled by stochastic bedrock landsliding

Authors: Robert Emberson[1,2]*, Niels Hovius[1,2], Albert Galy[3] and Odin Marc[1,2]

Affiliations:

[1] GFZ Deutsches GeoForschungZentrum, Potsdam, Germany

[2] Institute of Earth and Environmental Science, University of Potsdam, Germany

[3] CRPG-CNRS-UL, Nancy, France

*Correspondence to: robert.emberson@gfz-potsdam.de

A link between chemical weathering and physical erosion exists at the catchment scale over a wide range of erosion rates[1,2]. However, in mountain environments, where erosion rates are highest, weathering may be kinetically limited[3,4,5] and therefore decoupled from erosion. In active mountain belts, erosion is driven by bedrock landsliding[6], at rates that depend strongly on the occurrence of extreme rainfall or seismicity[7]. Although landslides affect only a small proportion of the landscape, bedrock landsliding can promote the collection and slow percolation of surface runoff in highly fragmented rock debris and create favourable conditions for weathering. Here we show from analysis of surface water chemistry in the Southern Alps of New Zealand that weathering in bedrock landslides controls the variability in solute load of these mountain rivers. We find that systematic patterns in surface water chemistry are strongly associated with landslide occurrence at scales from a single hillslope to an entire mountain belt, and that landslides boost weathering rates and river solute loads over decades. We conclude that landslides couple erosion and weathering in fast-eroding uplands and, thus, mountain weathering is a stochastic process that is sensitive to climatic and tectonic controls on mass wasting processes.

Exposure of fresh rock surfaces by erosion promotes efficient chemical weathering[8], but in active mountain belts with ample bedrock outcrop and mobile sediment, chemical weathering is strongly limited by the kinetics of mineral dissolution[9] and fluid travel times[10]. These are not strongly coupled with erosion rates, and little spatial variability in the solute load of mountain rivers is therefore expected. Nevertheless, mountain weathering rates vary widely[2] and can reach high values[2]. This could be

because locally high denudation rates can engender extremely fast soil production[11] and/or slow water circulation, with efficient solute release, but on fast eroding mountains, soils are mostly thin and discontinuous, and steep bedrock hillslopes promote efficient drainage. Instead, we propose that localized weathering is associated with deep-seated landsliding to which these slopes are prone. Exposure of fresh rock surfaces by erosion promotes efficient chemical weathering[8]. Bedrock landslides generate fresh surfaces in erosional scars, and potentially more importantly by intense fragmentation of mobile rock mass[12]. Moreover, they introduce concavity into hillslopes, which acts to catch and funnel precipitation and runoff into debris with limited hydraulic conductivity[13], thus allowing percolating water to react efficiently with the unweathered rockmass.

To determine the role of landslides in localizing and facilitating chemical weathering, we have measured surface water chemistry in the western Southern Alps (WSA) of New Zealand. There, high erosion rates (9±4mm/yr) are driven by landsliding[3] due to rapid rock uplift[14,15] on the Alpine fault (Fig. 1), combined with orographically forced precipitation averaging 7m/year[16]. The Southern Alps rise to 3754m, with mean catchment elevations of c.900-1000m. Dense vegetation covers slopes below about 1250m[17] but glaciers extend lower in three central catchments. The anthropogenic imprint on this landscape is slight.

The distribution of landslides in the WSA is well documented from remotely sensed images. Airphoto-based landslide inventories cover the period from 1935 to 2002[6,18] in approximately ten-year increments. We mapped subsequent landslides from Landsat 8 images taken in 2014. Together, these inventories contain about 4500 landslides, ranging in area from c.10^2m^2 up to 1.02x10^6m^2, with a mean of 1.18x10^4m^2. These landslides affected 2.1% of the total mapping area of about 2500km^2 and between 0.96% and 13.1% of individual catchment areas. Many landslides collect surface drainage from a larger upslope area. From a 30m resolution ASTER DEM, we estimate that on average the

upslope area is 4-5 times greater than the landslide area (Fig. S3) and the effective area drained through mapped landslides is 1-35% of total catchment area for landslides since 1980, and 2-40% for landslides since 1935.

If landslides are important seats of weathering in the WSA, then this should give rise to marked variability of local weathering, and a link between the degree of weathering and landsliding at the catchment scale. To test this, we collected water from seepage at the base of landslide deposits, runoff from nearby small (<1km^2) catchments without signs of recent mass wasting, and all major streams draining the mountain belt to the west, near the mountain front (Fig. 1). Spot sampling is likely representative of the river chemistry as total dissolved solids (TDS) values in individual WSA rivers only vary by 25% across a large range of discharge[2]. Lack of rain prior to and during sampling meant that landslide scarps were dry, but persistent seepage from landslide debris suggested a low hydraulic conductivity of these deposits. Seepage from two larger landslides of 1.67x10^{4}m^2 (Haremare creek, Fig. S1) and 3.18x10^{5}m^2 (Gaunt creek) and a series of smaller slides of 1.5-2.5x10^{3}m^2 (Jackson Bay) was sampled in detail. The first two sites are set in quartz-feldspar-biotite schists, in the immediate hanging wall of the Alpine fault[19], representative of the carbonate-poor metasedimentary rocks of the Southern Alps. The Jackson Bay landslides occurred in quartz-rich greywacke/argillite of the Australian Buller terrane[20] west of the fault.

In our samples, TDS concentrations are closely tied to geomorphic characteristics. In landslide seepage TDS values range from 2630 to 9840µmol/l, much higher than the 293-800µmol/l measured in runoff from catchments without landslides (Fig. 2) and also systematically higher than in the local stream water collected downstream, by a factor of at least 1.4 (Haremare creek) and up to 13 (Gaunt creek). The difference in lithology between

the WSA and Jackson Bay is expressed as variable Mg^{2+}/K^{+} in the dissolved load (Tables S1, S3), but the elevated TDS in landslide seepage is systematic across all sites.

Measured TDS values of WSA rivers plot on a mixing line between dilute runoff from soil covered slopes and concentrated landslide seepage (Fig. S2), suggesting that other solute inputs may be limited. Groundwater with residence times of weeks to months can contribute significantly to the solute flux from mountain belts[21,22], and landslide seepage is likely to be an important source. More than 80% of visited landslides had running seeps despite a relative drought prior to sampling. The solutes in this seepage come from the landslides themselves; elemental ratios indicate that they are not due to either hydrothermal input (Na^{+}/Ca^{2+} ratios are c.0.02-0.1 for landslide seeps, and c.10 for hydrothermal springs – tables S2 & S3, Fig S2) or other deep groundwater; monitored groundwater wells within the area[23,24] have Na^{+}/Ca^{2+} ratios between 0.29 and 0.8. Moreover, runoff in catchments without landsliding – which should also incorporate deep groundwater – have low TDS values (c.600µmol/l). Thus, our results suggest that weathering in the rapidly eroding WSA is significantly localised in recent landslides, giving rise to strong variations in solute concentrations in (near) surface water on length scales as small as 10^{1}m.

We have used the ensemble volume of mapped landslides to assess their importance in setting whole-catchment solute outputs. The volume of landslides per catchment, calculated with a regional area-volume relationship[25], was normalised by the catchment area, to yield a catchment landslide erosion rate, LS_{norm}, for a given interval. This has also allowed us to assess how landslide age can affect the river solute load. For 19 sampled rivers, the measured TDS_{modern} correlates with the logarithm of LS_{norm} in the catchment. The period 1980-2014 correlated best, with R^2 of 0.88 and Kendall's-Tau (hereon K-Tau) of 0.74 (Fig.3). For this interval, TDS values systematically range from 500-1800µmol/l for catchments with LS_{norm} from c.$10^{3}m^{3}/km^{2}$ up to $10^{5}m^{3}/km^{2}$ (Fig.3). Spot

samples taken from some of these rivers in 2000[26] show similar correlation with LS_{norm} for 1973-2002 (also three decades prior to sampling) (Fig.3), providing further support for our result.

The TDS_{modern} – Ls_{norm} relation suggests that spatial variability in river solute flux is determined by landslide weathering, which overprints a background set by baseflow and surface runoff. A two-endmember mixing model suggests that landslide seepage on average supplies 42% of solutes (Table S6, Fig. S4) from about 10% of the water flux in sampled rivers. This is in agreement with the calculated fraction of catchment area drained through landslides. At low flow conditions like those sampled we anticipate that slower seepage will form a greater part of the solute budget. For catchments with the greatest landslide volume, associated seepage contributes as much as 80% of the river dissolved load from 35% of the water flux, while in catchments with least landsliding, its contribution to the weathering flux can be negligible. It is likely that at low flow conditions like those sampled, slow seepage from landslides and other groundwater sources will form a greater part of the solute budget.

Data scatter may be caused by variable river dilution due to occasional precipitation during sampling, the range of landslide ages across the region, as discussed below, and the different relative distributions of landslide sizes, where some catchments have a few large slides and others have a similar ensemble landslide volume from many smaller slides. The log-linear relationship between catchment landslide volume and river solute load may result from a combination of effects; larger landslides have deeper scars and thicker deposits. Their volume does not scale linearly with the area of the scar[25] or the drained area (see methods) and, therefore, with the amount of precipitation collected. Percolation of water through a slide may also decrease with depth of deposit. Finally, deeper, fresher material, mined by larger landslides, is less likely to be fractured by near

surface effects[27] and so the internal surface area may also not scale linearly with landslide volume.

The weathering boost caused by exposure of fresh mineral surfaces should decay as landslide deposits age. This is supported by a comparison of the chemistry of seepage from landslides with known age with the average composition of surface runoff from catchments without landslides. The high $Ca^{2+}/(Na^{+}+Si+Ca^{2+})$ signature specific to landslides progressively decays from the youngest sampled slides, < 5 years, to values indistinguishable from surface runoff in a 60 year old landslide (Fig. S5). Also, the strength of fit between LS_{norm} and TDS_{modern} generally decreases for older landslide inventories (Table S7), despite important temporal variations in landslide rates (Fig. S6). The strongest correlation with river TDS_{modern} is obtained when all landslides since 1980 are combined. Thus, the very high landslide rates during 1980-1985 still disproportionately affect the river chemistry, and the effect of the degradation of these older slides on weathering is less than that of the order-of-magnitude drop in landslide rate since then. Nevertheless, the weaker correlation between river TDS_{modern} and landslide rates prior to 1980 indicates that the landslide weathering boost dissipates on decadal time scales. Both lines of evidence suggest that, in the WSA, the timescale over which landslides affect the weathering budget is about 30-60 years.

High measured $Ca^{2+}/(Na^{+}+Si+Ca^{2+})$ implies a high proportion of carbonate weathering in the landslides, but Silicon concentrations approximately double over the observed range of catchment landslide volumes. This implies that in steep, fast eroding uplands where landsliding is dominant, erosion and silicate weathering-driven CO_2 drawdown are coupled albeit with limited efficiency. The impact of landsliding on silicate weathering fluxes is further constrained by the small fraction of landscape area impacted by the process at a given time.

Our data show that landslides, with associated expansive mineral surface area in debris and extended, slow hydrological pathways, provide an optimal weathering environment, the volume of which is a first-order control on the dissolved load of rivers draining the WSA. Where bedrock-involved landsliding dominates, it provides an effective link between physical erosion and chemical weathering. The temporal and spatial stochasticity of landslide-driven erosion will be reflected in the weathering budget, and can explain the major part of spatial and temporal variability of solute transport in mountain rivers. Distributed weathering at sites not recently affected by landsliding appears to provide a steady input of solutes to mountain rivers, to which landslides add concentrated seepage for a period of decades and in proportion to their cumulative volume in a catchment. We anticipate that measurements of the weathering budget of the Southern Alps, and similar settings like Taiwan and the Himalayas, will be susceptible to important influences from the stochastic drivers of mass wasting such as intense rain[28] or shallow earthquakes[29], as the increased solute input from landslides after such events is likely to decay well within their return time.

References and Notes:

1. C. S. Riebe, J. W. Kirchner, R. C. Finkel. Erosional and climatic effects on long-term chemical weathering rates in granitic landscapes spanning diverse climate regimes. *Earth Planet. Sci. Lett.* **224**, 547-562 (2004).
2. W. B. Lyons. Chemical weathering in high-sediment-yielding watersheds. *New Zealand. J. Geophys. Res.* **110**, F01008 (2005).
3. K. L. Ferrier, J. W. Kirchner. Effects of physical erosion on chemical denudation rates: A numerical modeling study of soil-mantled hillslopes. *Earth Planet Sci. Lett.* **272**, 591-599 (2008).
4. G. E. Hilley, C. P. Chamberlain, S. Moon, S. Porder, S. D. Willett. Competition between erosion and reaction kinetics in controlling silicate-weathering rates. *Earth Planet. Sci. Lett.* **293**, 191–199 (2010).
5. J. L. Dixon, A. S. Hartshorn, A. M. Heimsath, R. A. DiBiase, K. X. Whipple. Chemical weathering response to tectonic forcing: A soils perspective from the San Gabriel Mountains, California. *Earth Planet. Sci. Lett.* **323-324**, 40-49 (2012).
6. N. Hovius, C. Stark, P. Allen. Sediment flux from a mountain belt derived by landslide mapping. *Geology*. **25**, 231–234 (1997).
7. S. Dadson, N. Hovius, H. Chen, W. Dade. Links between erosion, runoff variability and seismicity in the Taiwan orogen. *Nature*. **426**, 648–651 (2003).
8. Y. Huh, J. Edmond. The fluvial geochemistry of the rivers of Eastern Siberia: III. Tributaries of the Lena and Anabar draining the basement terrain of the Siberian Craton and the Trans-Baikal Highlands. *Geochim. Cosmochim. Acta*. **63**, 967–987 (1999).

9. A. J. West, A. Galy, M. Bickle. Tectonic and climatic controls on silicate weathering. *Earth Planet. Sci. Lett.* **235**, 211–228 (2005).

10. K. Maher, C. P. Chamberlain. Hydrologic Regulation of Chemical Weathering and the Geologic Carbon Cycle.

Science. **343**, 1502-1504 (2014)

11. I. J. Larsen et al. Rapid Soil Production and Weathering in the Southern Alps, New Zealand. *Science*. **343**, 637–640 (2014).

12. T. R. Davies, M. J. McSaveney. The role of rock fragmentation in the motion of large landslides. *Eng. Geol*. **109**, 67–79 (2009).

13. H. Lo, P. Chou, S. Hsu, C. Chao, C. Wang. Using Borehole Prospecting Technologies to Determine the Correlation between Fracture Properties and Hydraulic Conductivity : A Case Study in Taiwan. *J. Environ. Eng. Geophys*. **17**, 27–37 (2012).

14. J. Tippett, P. Kamp. Fission track analysis of the late Cenozoic vertical kinematics of continental Pacific crust, South Island, New Zealand. *J. Geophys. Res.* **98**, 16119–16148 (1993).

15. W. B. Bull, a F. Cooper. Uplifted Marine Terraces Along The Alpine Fault, New Zealand. *Science*. **234**, 1225–8 (1986).

16. R. Henderson, S. Thompson. Extreme rainfalls in the Southern Alps of New Zealand. *J. Hydrol. (NZ).* **38**, 309–330 (1999).

17. P. Bellingham, S. Richardson. Tree seedling growth and survival over 6 years across different microsites in a temperate rain forest. *Can. J. For. Res.* **918**, 910–918 (2006).

18. R. G. Hilton, P. Meunier, N. Hovius, P. J. Bellingham, A. Galy. Landslide impact on organic carbon cycling in a temperate montane forest. *Earth Surf. Process. Landforms*. **36**, 1670–1679 (2011).

19. R. Grapes, T. Watanabe. Metamorphism and uplift of Alpine schist in the Franz Josef-Fox Glacier area of the Southern Alps, New Zealand. *J. Metamorph. Geol.* **10**, 171–180 (1992).

20. C. J. Adams. Rb□Sr age and strontium isotope characteristics of the Greenland Group, Buller Terrane, New Zealand, and correlations at the East Gondwanaland margin. *New Zeal. J. Geol. Geophys.*, **47**, 189–200 (2004).

21. D. Calmels, A. Galy, N. Hovius, M. Bickle, A. J. West, M. Chen, H. Chapman. Contribution of deep groundwater to the weathering budget in a rapidly eroding mountain belt, Taiwan. *Earth Planet. Sci. Lett*. **303**, 48-58 (2011).

22. C. Andermann, L. Longuevergne, S. Bonnet, A. Crave, P. Davy, R. Gloaguen. Impact of transient groundwater storage on the discharge of Himalayan rivers. *Nat. Geosci*. **5**, 127-132 (2012).

23. GNS Science, 2015. GNS Science Geothermal and Groundwater Database, http://ggw.gns.cri.nz/ggwdata/, last accessed 03/08/2015.

24. S. Cox, C. Menzies, R. Sutherland, P. H. Denys, C. Chamberlain, D. A .H. Teagle. Changes in hot spring temperature and hydrogeology of the Alpine Fault hanging wall, New Zealand, induced by distal South Island earthquakes. *Geofluids*, **15**, 216-239 (2015).

25. I. J. Larsen, D. R. Montgomery, O. Korup. Landslide erosion controlled by hillslope material. *Nat. Geosci*. **3**, 247–251 (2010).

26. A. D. Jacobson, J. D. Blum, C. P. Chamberlain, D. C. Craw, P. O. K. Koons. Climatic and tectonic controls on chemical weathering in the New Zealand Southern Alps. *Geochemica Cosmochim. Acta*. **67**, 29–46 (2003).

27. K. Leith, J. R. Moore, F. Amann, S. Loew. In situ stress control on microcrack generation and macroscopic extensional fracture in exhuming bedrock. *J. Geophys. Res. Solid Earth*. **119**, 594–615 (2014).

28. T. Glade. Establishing the frequency and magnitude of landslide-triggering rainstorm events in New Zealand. *Environ. Geol*. **35**, 160–174 (1998).

29. N. Hovius et al. Prolonged seismically induced erosion and the mass balance of a large earthquake. *Earth Planet. Sci. Lett*. **304**, 347–355 (2011).

Acknowledgments:

We thank the New Zealand Department of Conservation for permission to sample the field sites (Authority number 38154-RES); A. Golly for assistance in the field; and Robert Hilton, A. Joshua West and Christian France-Lanord for discussion. Sample analysis was carried out in the GFZ HELGES lab with assistance from Jan Schuessler and Carolin Zorn. Arjun Heimsath and two anonymous reviewers provided advice which greatly improved the manuscript.

Author Contributions

R.E., N.H. & A.G. conceived the study and collected the samples; R.E. carried out lab analysis and data processing of chemical samples. O.M. completed the landslide data and calculated volumes; R.E. wrote the paper with significant input from all other authors.

Additional Information

The authors declare no competing financial interests. The data reported in this submission are fully available in the online supplementary material. Please address all correspondence to R.E.: robert.emberson@gfz-potsdam.de.

Figure Captions

Fig. 1. Study area in the western Southern Alps, with catchment outlines and sampling locations for rivers, landslides and hot springs. Landslides were sampled in detail at three sites: A – Haremare Creek; B – Gaunt Creek; C – Jackson Bay. Catchments where a lack of imagery prevented complete mapping of landslides are shown with a star.

Fig. 2. TDS values for major rivers (Rivers), runoff from catchments unaffected by landsliding (Runoff), landslide springs (S) and their local stream water (L); A – Haremare Creek, B – Gaunt Creek, C – Jackson Bay. Note starred river samples taken where landslides were not mapped due to lack of imagery.

Fig. 3. Total Dissolved Solids concentrations measured in rivers in February 2014 plotted against the normalised landslide volumes (m^3 of landslide per km^2) in their catchment for the landslide interval 1980-2014. Also shown is the river chemistry data of Jacobson et al. 2003[26], plotted against normalized landslide volumes for 1973-2000. The log-linear best fit and accompanying 1 standard deviation range are calculated for our data only. Horizontal error bars are 95% confidence intervals for volumes; vertical error bars represents the total uncertainty on measurement of the spot samples. Circular symbols are rivers without significant glaciers; squares include glaciers.

Methods

Sampling and Analytical Methodology

Samples were collected after three relatively dry weeks with approximately half the monthly average precipitation[30]. Under these conditions, dilution of surface waters due to direct runoff of rainfall is limited. Despite the lack of significant recent rainfall, springs were found at the base of about 80% of visited landslides, suggesting that many landslides in the WSA are unlikely to ever be dry. Landsliding is prevalent across the mountain belt but several of the sampled sites coincide with faults where springs could have a hydrothermal source. To evaluate this, hot spring water was sampled at four locations within the WSA (Fig. 1).

All water samples were collected using an HDPE syringe, filtered on site using single-use 0.2µm PES filters into several HDPE bottles thoroughly rinsed with filtered sample water for different analyses. Samples for cation analysis were acidified using ultrapure HNO_3^-. pH values were measured in the field at the time of sample collection. Analysis of cations was carried out using a Varian 720 ICP-OES, using SLRS-5 as an external standard, and GFZ-RW1 as an internal standard and quality control (QC). QC samples were included for every 10 samples to account for drift; no systematic drift was found, with random scatter less than 5%. Sample uncertainties were determined from calibration uncertainties, and were always lower than 10% (Ca^{2+}: 4%; K^+: 4%; Mg^{2+}: 4%; Na^+: 10%; Si: 8%, Sr^{2+}: 2%). Anion analysis was performed using a Dionex ICS-1100 Ion Chromatograph, using USGS standard M206 (Spring 13) as external standard and QC. Uncertainties were always less than 10% for each of the major anions (Cl^- and SO_4^{2-}). Bicarbonate (HCO_3^-) was calculated by charge balance; Nitrate (NO_3^-) was negligible in all the measured samples.

Correction for atmospheric input

Cyclic salt dissolved in rain can impact the total dissolved load measured in river waters, and must be removed to observe true effects from weathering. This can be done using spot samples or seawater ratios as an approximate estimate[26,31] but we preferred using volume-weighted average rainfall chemistry from the MaiMai catchment (also on the western side of the Southern Alps)[32] due to the similar setting and long term average – single samples might not accurately represent the reach over which incoming storms had travelled (and therefore the level of concentration vs. seawater).

Using the ratios of Cl^- to major cations (Ca^{2+}, K^+, Mg^{2+} and Na^+) and assuming all Cl^- results from cyclic contribution, we removed cyclic cation contributions using the following standard equation:

$$[X]_{cyclic} = [Cl^-]_{sample} \times ([X]_{rainfall}/[Cl^-]_{rainfall})$$

(Equation S1) where [X] is any of the measured concentration of cation. We appreciate that assumption of all Chloride resulting from seawater may be an overestimation, and we did not correct the hot spring samples since Chloride is at very high concentrations. The previous study of the MaiMai catchment did not measure SO_4^{2-} concentrations, so we followed an established protocol[2] in using the seawater ratio divided by 2.

The correction using the volume weighted average for the MaiMai catchment yielded results close to those obtained by other authors working in the same area[26,31] for the larger rivers within the mountain belt, but the samples collected in Jackson Bay were taken so close to the ocean (tens of metres) that this was not appropriate; the measured Chloride was so high (between 211 and 454 μmol/L) that in some cases negative results were obtained for concentrations of other solutes when rainwater ratios were used. For these samples we used seawater ratios for the major ions to correct for cyclic input.

Extent of Landslide Mapping

Although we took spot samples of the rivers all along the mountain front, from Hokitika to Jackson Bay, not all of those catchments had landslides mapped due to incomplete coverage of either aerial photographs or cloud-free satellite images; even since the advent of regular Landsat photography of the requisite detail level to map landslides (Landsat 5 and ASTER onwards) there are no cloud-free images of the Southern-most catchments (Haast, Okuru, Turnbull, Waiatoto and Arawhata rivers) until very recently (Landsat 8 onwards – 2013-2014) which precludes obtaining the local landslide rates over the period of interest.

Estimation of total landslide volume

We have used published area-volume relationships[25] to estimate the volume of landslides from their mapped areas. It was assumed that landslides with area > 10^5 m^2 involved bedrock, and that smaller landslides were mixed bedrock and soil failures. Our landslide maps don't distinguish between scar and deposit, lumping the two in one area measure. According to Larsen et al.[25], scars and deposits have area-volume relations with the same power-law exponent, implying constant size ratios between scar and deposit areas of 1.1 and 1.9 for mixed and bedrock landslides, respectively. Hence, we have estimated the scar area by dividing the mapped landslide area by 2.1 and 2.9 for mixed and bedrock landslides, respectively, assuming that runout was equal to the length of the affected area. This may lead to an overestimation of landslide scar volume where runout was much longer, mostly for small slides, which do not contribute significantly to the total eroded mass. Conversely, some large landslides on gentle slopes have overlapping scar and deposit areas, meaning that our correction causes a significant underestimation of the scar size and thus the landslide volume. As a systematic way to constrain runout variations is not available, we have applied a blanket correction for every slide, thus obtaining a conservative total volume. We have calculated the volume of every individual landslide, and summed to obtain a total volume of landslides for a catchment and/or mapping interval. Uncertainties in this approach include the coefficient and exponent of the landslide area-volume relations, $V = \alpha A^{\gamma}$, for which standard deviations have been reported as $\sigma_\gamma = \sigma_\alpha = 0.005$ for mixed bedrock-soil landslides and $\sigma_\gamma = 0.02$ and $\sigma_\alpha = 0.03$ for bedrock landslide scars[25], and mapping errors for which we have assumed a standard deviation of 20% of the mapped area. These uncertainties were propagated into our volume estimates using a Gaussian distribution. The standard deviation on the total landslide volume for a catchment or interval was calculated assuming that the volume of each individual landslide was unrelated to that of any other, thus, ignoring possible co-variance. Hence, the total volume uncertainty depends heavily

on the size distribution of landslides. When the total landslide volume is dominated by the many medium sized landslides in a population, then the uncertainty on the total volume estimate is small, because it is unlikely that all important individual landslides are biased in the same way. However, when the total volume is dominated by a few very large landslides, then the uncertainties on their volumes are less likely to cancel out, which leads to a large uncertainty on the total volume estimate.

Estimation of area draining into landslides

We calculated the upslope areas draining into each landslide using the 30m ASTER DEM of the WSA. The area calculated is the number of DEM cells from where the downstream flow path intersects a mapped landslide, plus the area of the landslide itself, calculated using the FLOWobj d8 routing algorithm available in the Topotoolbox-2.0.1 release for MATLAB. These areas are summed for each catchment and then compared with the total area of the catchment. To avoid double-counting overlapping upslope areas for landslide catalogues of different ages each DEM pixel is only counted once for the purposes of total upslope area. The upslope area draining into landslide deposits constitutes 8.7% of the WSA landscape, ranging from 1% to 34% among the sampled catchments for landslides that occurred after 1980. This increases to 2.8-40% for the entire 70 year landslide catalogue. Figure S3 shows an example of the processed DEM. We acknowledge that any estimates of fluxes based on drained area are an upper limit on the water flowing through these landslide springs.

Estimation of end-members and fluxes

Estimation of the proportional landslide weathering input to river solute load requires definition of end members. As stated in the main text, we use landslide springs and runoff, both of which have a wide range of measured values, the choice of which will influence the relative fractions of the sources in the final result. We therefore calculate mixing proportions for each river using the mean of our measured samples. The range is one standard deviation. Landslide springs: 5820µmol/l ± 2293µmol/l. Runoff: 576µmol/l ± 150µmol/l. Note that we did not use samples collected in Jackson Bay for these end member estimates, as although they display the same systematic increase in TDS in the landslide springs, the different lithology of the Australian plate has a strong control on the actual values of TDS; therefore actual values of TDS are not comparable. However the samples collected from the rest of the WSA all drain the same lithology and as such are comparable.

We can compare the estimates of solute flux from these end-members to the estimated water flux through landslides from the calculated upstream collection areas. The proportion of runoff that passes through the landslides tends to be higher when the end members and measured river concentrations are used to calculate proportions than when using upstream area of landslides to estimate the flux; however, the same pattern emerges. The period of sampling was during a drier-than-average period in the WSA, and it is not surprising that the landslide component should be over represented in the rivers during the sampling period, since this is a slower path for solutes, as evidenced by the continued flux from these sources despite the lack of rainfall.

Table S6 contains all calculated data for solute flux, water flux, landslide areas and volumes for all catchments in question.

Although the estimates of water fluxes based on end-member contributions and those based on calculations of upstream areas broadly agree, there are important differences; in particular, the upstream area calculations for several of the catchments where landslide volumes are low exceeds the required flux based on end-member calculations, whereas for some of the rivers with higher TDS values, the flux based on upstream-area underestimates the end-member requirement. We likely overestimate the water entering the smaller landslides which proportionally make up a greater part of the volumes in the catchments with lower TDS, while likely underestimate the flux from large landslides where more water may be stored and at low-flow sampling conditions give rise to higher concentrations. Very large landslides dominate the volumetric contribution from landslides in the Cook, Poerua and Waitaha rivers, and thus upstream area to volume ratios are smaller. We also note that the McDonald Creek has a higher flux from landslides than expected from concentration, but this river drains mostly glacial till; the landslides are systematically smaller within the catchment, but generate a disproportionally large upstream area. This leads to an overestimate of flux. Despite these caveats, the estimates of fluxes still broadly agree. This is demonstrated in Figure S4, where upstream area is calculated for each catchment and compared with the TDS. The relationship is similar to the volume / TDS relationship, with the notable exception of the catchments mentioned above. No error bars are plotted for the upstream area calculation since we have not quantified the error on these measurements.

Landslide ages and chemical decay time

At 13 sampling points split between eight locations (Table S5), landslide seepage has been sampled where the age of the landslide is well constrained from satellite images or aerial photographs. With these samples, we are able to show how the increased solute output from landslides decays with time. We have compared the chemistry of the landslide seepage with a mountain-belt wide average of surface runoff composition – an average of water from small streams draining sub-catchments without recent landslide activity. This is the same surface runoff end-member signature we defined in the mixing calculations above. Simple TDS values might not account for local differences between landslides, for example, how much rainfall might have fallen on each one recently. Therefore, we used specific chemical ratios to isolate the chemical effect of landslide aging. Since trace carbonate in landslides is weathered out first, resulting in an excess in Ca^{2+} vs other weathering products, it is informative to look at the ratio of Calcium to other major weathering products (since Calcium is also the major cation in the solute budget, this represents the majority of the excess weathering from the landslides) – i.e. $Ca^{2+}/(Ca^{2+}+Na^{+}+Si)$ – in the landslide seepage as compared to the ambient surface runoff.

Landslide size is not considered in this preliminary analysis of chemical landslide aging, but the trend in Figure S5 independently supports our observations on the time-dependent strength of the relationship between TDS and LS_{norm} from which we infer that landslides boost weathering for 30-60 years after failure.

The strength of this boost decreases with time, meaning that the impact of older landslides on river chemistry is likely to be swamped by that of younger landslides. Full data for these landslides is found in Table S5.

This combines well with the comparison of changes in correlation between TDS and volumes; as discussed in the main text, the correlation peaks for the last 35 years of landsliding, primarily due to the high rates between 1980-1985; the fall in correlation later on indicates that the older landslides are no longer having a strong effect. The values for R^2 and K-Tau are shown in Table S7, and the changing rate of landsliding over the last 70 years is shown in Figure S6. Data collected by Jacobson et al.[26] in 2000 also has a peak in correlation 30 years prior to it's sampling, although the peak correlation is when all of the landslides are considered as a whole. The landslides mapped between 1940 and 1948 show a similar spatial distribution to those between 1980-1985, so this increase in correlation for the full landslide catalogue is likely to reflect this rather than any long lasting impact of the landslides between 1940 and 1948.

References - Methodology

30. New Zealand National Climate Database, www.cliflo.niwa.co.nz, last accessed 15/01/2015.

31. J. Moore, A. D. Jacobson, C. Holmden, D. Craw. Tracking the relationship between mountain uplift, silicate weathering, and long-term CO2 consumption with Ca isotopes: Southern Alps, New Zealand. *Chem. Geol.* **341**, 110-127 (2013).

32. W. Verhoeven, R. Herrmann, R. Eiden, O. Klemln. Theoretical and Applied Climatology A Comparison of the Chemical Composition of Fog and Rainwater Collected in the Fichtelgebirge, Federal Republic of Germany, and from the South Island of New Zealand. *Theor. Appl. Climatol*. **38,** 210-227 (1987).

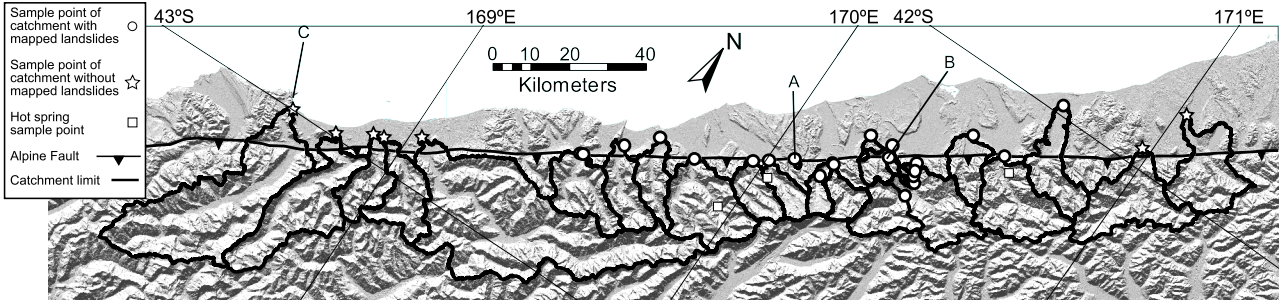
Sample point of catchment with mapped landslides
Sample point of catchment without mapped landslides
Hot spring sample point
Alpine Fault
Catchment limit
43ºS
169ºE
170ºE
42ºS
171ºE
0 10 20 40
Kilometers
N
A
B
C

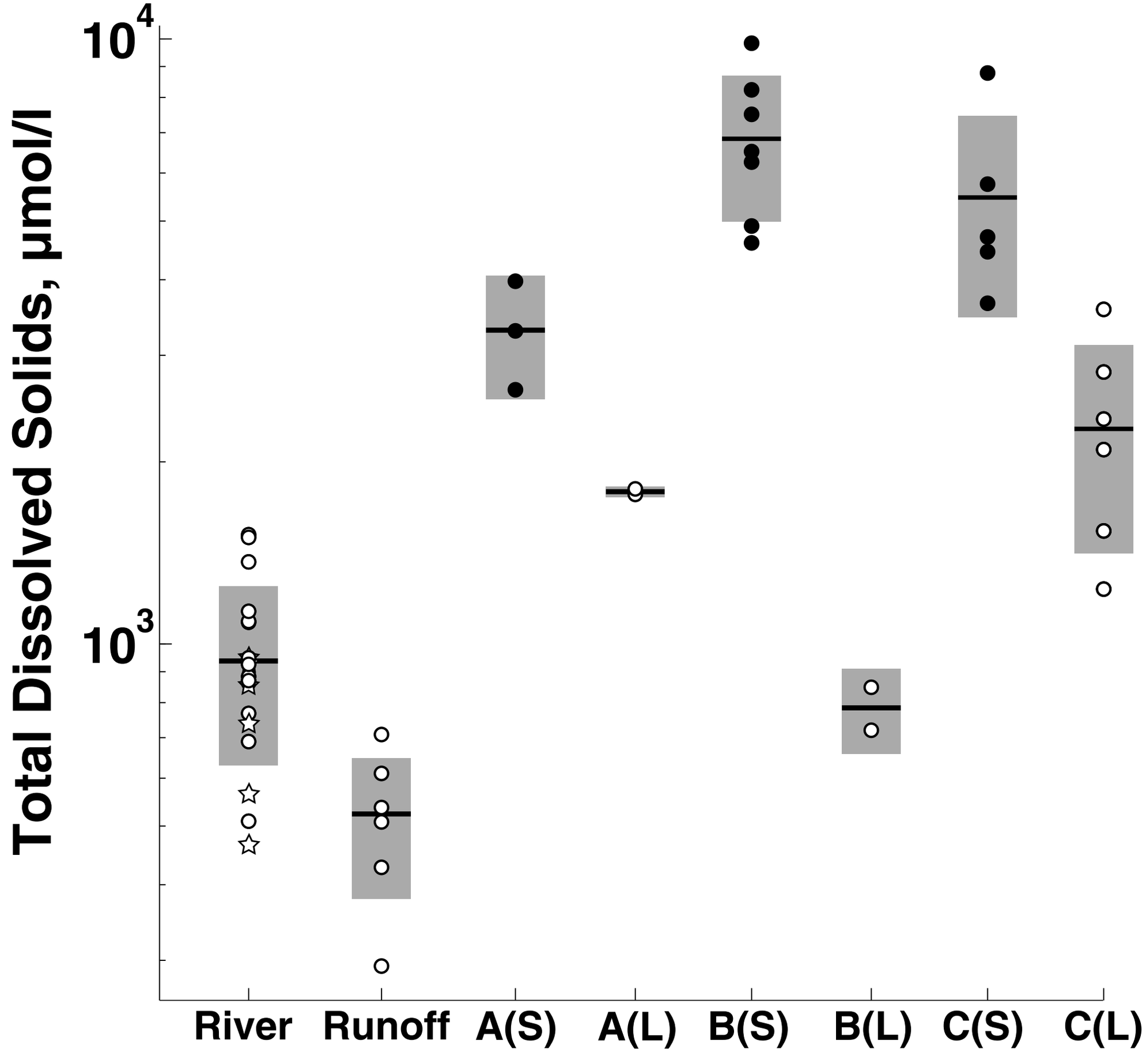
Total Dissolved Solids, µmol/l
10^4
10^3
River
Runoff
A(S)
A(L)
B(S)
B(L)
C(S)
C(L)

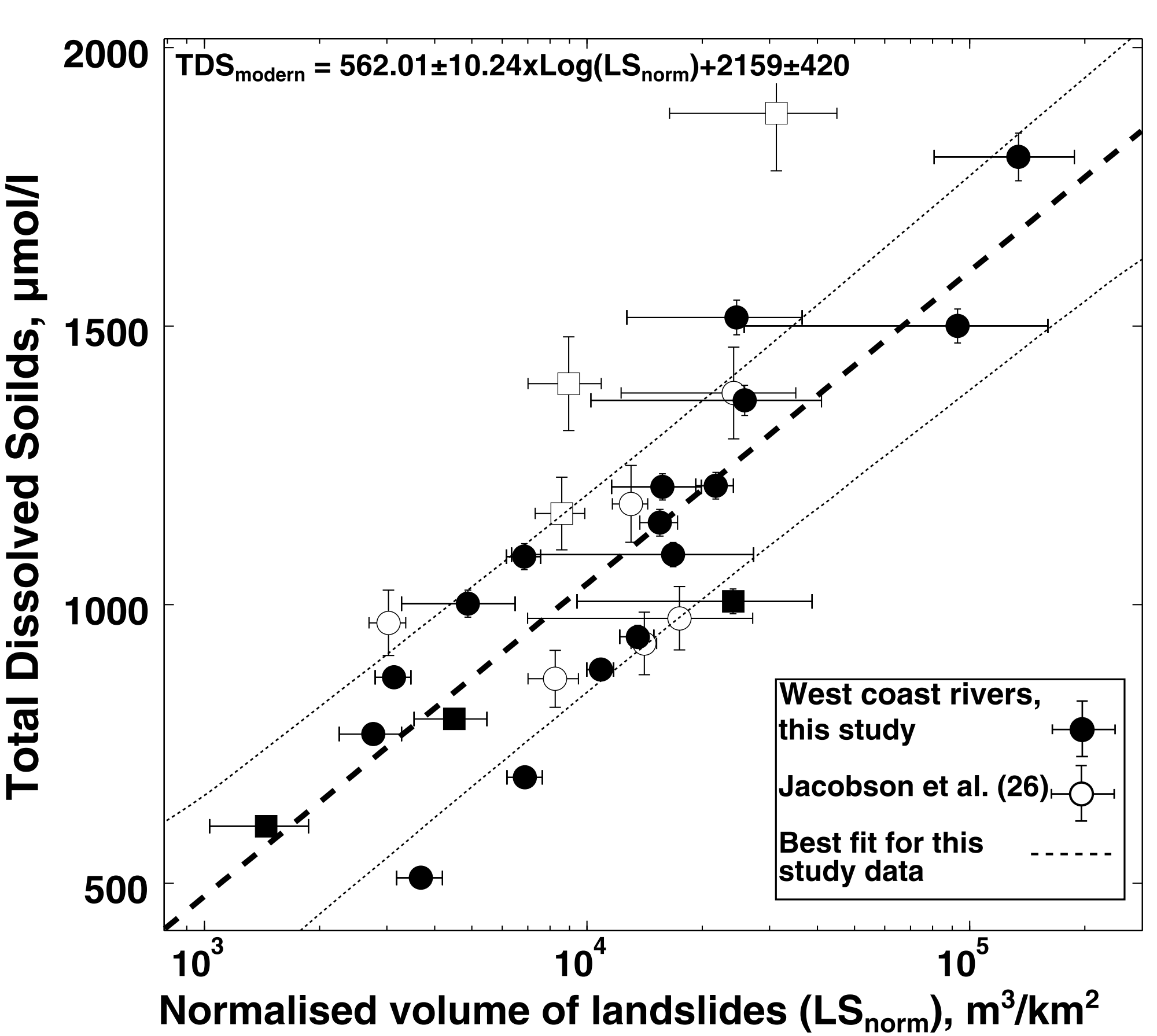
TDS$_{modern}$ = 562.01±10.24xLog(LS$_{norm}$)+2159±420
2000
1500
1000
500
Total Dissolved Soilds, µmol/l
10^3
10^4
10^5
Normalised volume of landslides (LS$_{norm}$), m^3/km^2
West coast rivers, this study
Jacobson et al. (26)
Best fit for this study data